Proceedings of the 7th International Symposium on Cavitation
CAV2009
August 17-22, 2009, Ann Arbor, Michigan, USA

CAV2009 – Paper No. 46

Modeling and analysis of a cavitating vortex in 2D unsteady viscous flow

Johan Bosschers
Maritime Research Institute Netherlands (MARIN)
Wageningen, the Netherlands

ABSTRACT

Two models, of which one analytical and the other computational, have been developed to describe an axi-symmetric cavitating vortex in two-dimensional, unsteady, incompressible and viscous flow. The models are used to investigate the influence of viscosity on the flow structure, cavity size and cavity resonance frequency. The analytical formulation is an extension of the Lamb-Oseen vortex and has not been presented before. It is derived under the assumption of small radial velocity equivalent to small temporal changes of the cavity diameter. The computational model solves the equations without simplifications. It is shown that viscous effects have a significant influence on cavity radius and resonance frequency if the cavity size is on the same order or smaller than the viscous core size.

INTRODUCTION

Cavitating vortices are relevant as an acoustic source mechanism as it may cause noise and vibration on board a ship and it contributes to the ship acoustic signature [1]. The dynamic behavior of a cavitating vortex without collapse can be modeled in potential flow by a dispersion relation for the perturbations of the cavitating core [2, 3, 4]. Comparison between theoretical and experimental data for resonance wave length or frequencies shows qualitative agreement [2, 3, 4] with differences being attributed to, among others, viscous effects. The lack of information on the influence of viscous effects on cavitating vortices to substantiate this conclusion formed the motivation for the present work.

Velocity components in a tip vortex trailing of a wing of elliptical planform with and without cavitation were measured by Falcão de Campos (1992) [5] using Laser Doppler Velocimetry. It is concluded that further away from the cavity the velocity distribution for the non-cavitating vortex and the cavitating vortex is identical. The same conclusion is drawn by Rijsbergen & Kuiper (1997) [6] who also used LDV to measure the velocity structure for a hub vortex. The velocity distribution near the cavity could not be measured in detail due to the unsteadiness of the cavity.

Several investigations were made on finding the relation between the radius of the cavitating core r_c and cavitation number σ. Kuiper (1981) [7] matched the relation $\sigma \propto 1/r_c^p$ with experimental data to find the value for p equal to 1 for initial tests and equal to 0.5 for cases close to inception while $p = 2$ for potential flow. A similar scaling relation between the circumferential velocity and radius has been investigated in [6] using conservation of momentum and kinetic energy, but a good match with experimental data could not be obtained. Different heuristic modifications of a Lamb-Oseen vortex were investigated by Arakeri *et al* (1988) [8] and Choi & Ceccio (2007) [9], with the modification formulated such that it satisfies either zero shear stress or zero velocity at the cavity. Parameters were then tuned to match experimental data for the relation between r_c and σ. Similarity solutions for cavitating vortices in viscous flow were derived from the three-dimensional Navier-Stokes equations by Bosschers *et al* (2008) [10] and were found to exist only for parabolic growth of the circulation and the cavity core. The model can be used to locally match a cavitating leading edge vortex but the results could not be validated using experimental data.

The present work discusses the influence of viscous effects on cavitating vortices in two-dimensional axi-symmetric flow using two methods. Both methods are based on solutions of the Navier-Stokes equations and form an alternative to the heuristic formulations of [6, 7, 8, 9] and are more easily understood than the solution presented in [10]. The first method is an analytical solution derived under the assumption that the radial velocity of the cavity is much smaller than the circumferential velocity. The resulting formulation for the circumferential velocity is an extension of the formulation for the Lamb-Oseen vortex from which analytical expressions for the pressure and vorticity can

be derived. In the second method the equations are solved without simplifications using a computational procedure. This method is used to analyze the structure of a vortex with oscillating cavity without collapse. The boundary conditions at the cavity for both methods are derived from the jump relations similar to [10] and lead to a zero shear stress condition.

The analytical formulation and its results are new and have not been presented before. Results confirm experimental findings on the influence of viscous effects. The computational procedure and its results can be seen as an extension of the method and results presented by Chahine (1995) [11]. The detailed analysis of the influence of viscous effects on the resonance frequency of a 2D cavitating vortex presented here is new and explains some of the differences found between 3D potential flow theory and experiment as presented in [4]. All results are valid for laminar flow but can be extended to turbulent flow by using an appropriate value of the eddy viscosity.

ANALYTICAL SOLUTION: DERIVATION

The classical analytical solution for a vortex in two-dimensional viscous flow is the Lamb-Oseen vortex [12]. Here a similar type of solution is generated for a cavitating vortex. Consider the incompressible, axisymmetric unsteady continuity and Navier-Stokes equations in a cylindrical coordinate system (r,θ,z) with velocity components (u,v,w) in radial, circumferential and axial direction respectively. It is furthermore assumed that the flow is two-dimensional. Hence, the velocity in axial direction is constant and all derivatives in axial direction are zero. The resulting equations are given by

$$\frac{\partial u}{\partial r}+\frac{u}{r}=0 \tag{1}$$

$$\frac{\partial u}{\partial t}+u\frac{\partial u}{\partial r}-\frac{v^2}{r}=-\frac{1}{\rho}\frac{\partial p}{\partial r} \tag{2}$$

$$\frac{\partial v}{\partial t}+u\frac{\partial v}{\partial r}+\frac{uv}{r}=\frac{\mu}{\rho}\left(\frac{\partial^2 v}{\partial r^2}+\frac{1}{r}\frac{\partial v}{\partial r}-\frac{v}{r^2}\right) \tag{3}$$

The diffusion term in the radial momentum equation is identical to zero due to the formulation of the continuity equation.

The order of magnitude of each term in the equations is analyzed by introducing a perturbation parameter ε with respect to a reference circumferential velocity V and a reference radial length R and assuming that the radial velocity component is an order of magnitude smaller than the reference velocity. The velocities and coordinates then scale as

$$\begin{aligned} u &= \varepsilon V\hat{u} \\ v &= V\hat{v} \\ p &= \rho V^2\hat{p} \\ r &= R\hat{r} \\ t &= \hat{t}\,R/V \end{aligned} \tag{4}$$

Substitution of Eq. (4) in Eq. (1) through (3), assuming that $\rho VR/\mu = \mathrm{Re} = O(1)$ and neglecting all terms of order ε and smaller by the condition $\varepsilon << 1$ gives

$$\frac{\partial u}{\partial r}+\frac{u}{r}=0 \tag{5}$$

$$\frac{v^2}{r}=\frac{1}{\rho}\frac{\partial p}{\partial r} \tag{6}$$

$$\frac{\partial v}{\partial t}=\frac{\mu}{\rho}\frac{\partial}{\partial r}\left[\frac{1}{r}\frac{\partial(vr)}{\partial r}\right] \tag{7}$$

from which it is observed that the radial and circumferential velocity are decoupled and that the pressure only depends on the circumferential velocity.

The boundary conditions for the non-cavitating vortex at $r\to\infty$ are that the radial velocity equals zero and the circumferential velocity is described by a potential flow vortex with circulation Γ_∞

$$v=\Gamma_\infty/2\pi r \tag{8}$$

At the centre of the vortex, the radial velocity should be equal to zero which implies that the radial velocity is zero throughout the flow field. At the centre for the vortex, the circumferential velocity should be zero as well. The solution for the circumferential velocity is the Lamb-Oseen vortex given by

$$v=\frac{\Gamma_\infty}{2\pi r}\left[1-e^{-r^2/(4\nu_l t)}\right] \tag{9}$$

where ν_l corresponds to the kinematic viscosity. The boundary conditions for a cavitating vortex are given by the jump relations for mass and momentum. These jump relations are obtained using the Reynolds transport theorem for conservation of mass and momentum for the total volume of fluid and vapour with the boundary of the interface moving with relative velocity $\mathbf{u_s}$. The equations are given in vector format by

$$\left[\!\left[\rho(\mathbf{u}-\mathbf{u}_s)\cdot\mathbf{n}\right]\!\right]=0 \tag{10}$$

$$\left[\!\left[\rho\mathbf{u}\left[(\mathbf{u}-\mathbf{u_s})\cdot\mathbf{n}\right]-\bar{\boldsymbol{\tau}}\cdot\mathbf{n}\right]\!\right]=0 \tag{11}$$

in which surface tension has been neglected, $\mathbf{n}$ corresponds to the normal at the interface and $\bar{\boldsymbol{\tau}}$ to the stress tensor, given for incompressible flow by

$$\bar{\boldsymbol{\tau}}=-p\bar{\mathbf{I}}+\mu\left[\nabla\mathbf{u}+(\nabla\mathbf{u})^T\right] \tag{12}$$

The boundary conditions can be simplified by assuming that the density and molecular viscosity of water vapour is negligible small compared to the values of liquid and that the pressure inside the cavity equals vapour pressure p_v. The boundary conditions at the cavity are then given by:

$$u = u_s = \frac{d r_c}{dt} \tag{13}$$

$$p_c - 2\mu \frac{\partial u}{\partial r} = p_v \tag{14}$$

$$\frac{\partial v_c}{\partial r} - \frac{v_c}{r} = 0 \tag{15}$$

Eq. (15) states that the shear stress at the cavity equals zero. Integration of this equation reveals that the circumferential velocity at the cavity equals solid body rotation. Using the same order of magnitude analysis as discussed before gives for the normal stress boundary condition at the cavity, Eq. (14)

$$p_c = p_v \tag{16}$$

A general analytical solution for the circumferential velocity that satisfies Eq. (7) is given by

$$v = \frac{\Gamma_\infty}{2\pi r}\left[1 - \beta\, e^{-\zeta r^2 / r_{vw}^2}\right] \tag{17}$$

where β is an arbitrary constant whose value depends on the boundary condition at the inner edge of the flow field. Compared to Eq. (9), the exponent is rewritten by introducing a viscous core radius for non-cavitating (wetted) flow defined by $r_{vw} = \sqrt{4\nu_l \zeta t}$. The constant $\zeta = 1.2564$ is used so that the circumferential velocity has its maximum value at the viscous core for the non-cavitating vortex $\beta = 1$. Substitution of Eq. (17) in Eq. (15) gives

$$\beta = \frac{r_{vw}^2}{r_{vw}^2 + \zeta r_c^2} e^{\zeta r_c^2 / r_{vw}^2} \tag{18}$$

The requirement that β is a constant is only satisfied if

$$r_c = c_1 r_{vw} = 2c_1 \sqrt{\zeta \nu_l t} \tag{19}$$

with c_1 a (non-dimensional) proportionality constant. The formulation for the circumferential velocity of a cavitating vortex is now given by

$$v = \frac{\Gamma_\infty}{2\pi r}\left\{1 - \frac{r_{vw}^2}{r_{vw}^2 + \zeta r_c^2} \exp\left[-\zeta \frac{\left(r^2 - r_c^2\right)}{r_{vw}^2}\right]\right\} \tag{20}$$

from which the velocity v_c at the cavity radius can easily be obtained

$$v_c = \frac{\Gamma_\infty}{2\pi}\left(\frac{\zeta r_c}{r_{vw}^2 + \zeta r_c^2}\right) \tag{21}$$

Substitution of Eq. (20) in Eq. (6) and integration from radius r to infinity gives the formulation for the pressure

$$p - p_\infty = -\frac{\rho \Gamma_\infty^2}{(2\pi r)^2}\left\{\begin{array}{l} \frac{1}{2} - \beta e^{-\zeta r^2 / r_{vw}^2} + \frac{\beta^2}{2} e^{-2\zeta r^2 / r_{vw}^2} \\ + \frac{\beta \zeta r^2}{r_{vw}^2} E_1\left(\zeta r^2 / r_{vw}^2\right) \\ - \frac{\beta^2 \zeta r^2}{r_{vw}^2} E_1\left(2\zeta r^2 / r_{vw}^2\right) \end{array}\right\} \tag{22}$$

where $E_1(x)$ corresponds to the exponential integral. Substitution of the cavity radius where pressure equals vapour pressure prescribes the relation between cavitation number and cavity size. The minimum pressure in the center of the non-cavitating Lamb-Oseen vortex is given by

$$p_{\min} - p_\infty = -\frac{\rho \Gamma_\infty^2}{4\pi^2 r_{vw}^2}\, \zeta\, \ln 2 \tag{23}$$

Finally, the radial velocity component is obtained by combining Eq. (13) and (19) with Eq. (5) which results into

$$u = c_1 \frac{r_c}{r} \sqrt{\frac{\zeta \nu_l}{t}} = c_1^2 \frac{2\zeta \nu_l}{r} = \left(\frac{r_c}{r_{vw}}\right)^2 \frac{2\zeta \nu_l}{r} \tag{24}$$

The presented formulations are derived from the unsteady Navier-Stokes equations similar to the original derivation of the Lamb-Oseen vortex. However, alternative formulations for the (non-cavitating) Lamb-Oseen vortex have been presented in literature as well. For example, Newman (1959) [13] applied a small perturbation analysis for a trailing vortex using the stationary flow equations including an axial perturbation velocity which is small with respect to the axial reference velocity W. The expression for the circumferential velocity is then identical to Eq. (9) with the substitution $t = z/W$. The radial and axial velocity components are now coupled and involve an arbitrary constant which Newman relates to the viscous drag of the wing generating the trailing vortex. However, for a cavitating vortex no equivalent solution for the axial perturbation velocity could be found in the present study. Hence, for stationary flow the axial velocity should be constant (or the perturbation velocity should be of order ε^2) and the circumferential and radial velocity are given by Eq. (20) and Eq. (24) respectively.

ANALYTICAL SOLUTION: ANALYSIS AND RESULTS

The analytical solution shows a temporal growth of the cavity radius and viscous core radius due to diffusion. However, the results also lead to a temporal variation of the pressure difference between the cavity and the position at infinity which does not seem realistic from a physical point of view. The temporal behavior should therefore be considered with care and will be further investigated using the computational procedure in the second part of the paper. The results for the circumferential velocity and pressure are valid

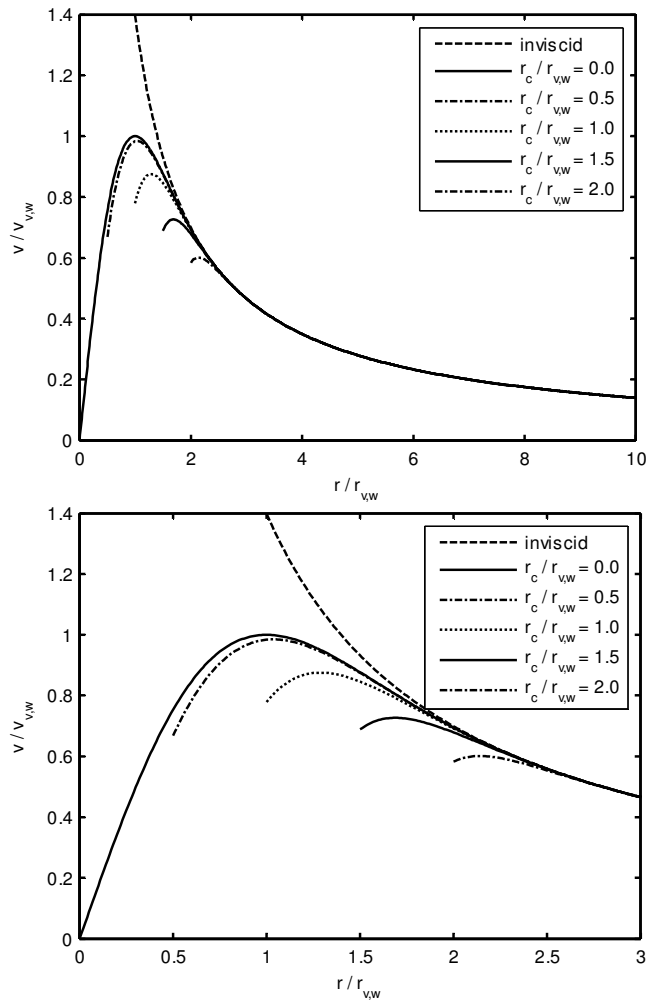

Figure 1: Non-dimensional circumferential velocity distribution given by Eq. (20) for various non-dimensional cavity radii. Top figure shows the overall distribution, bottom figure shows a zoom near the centre.

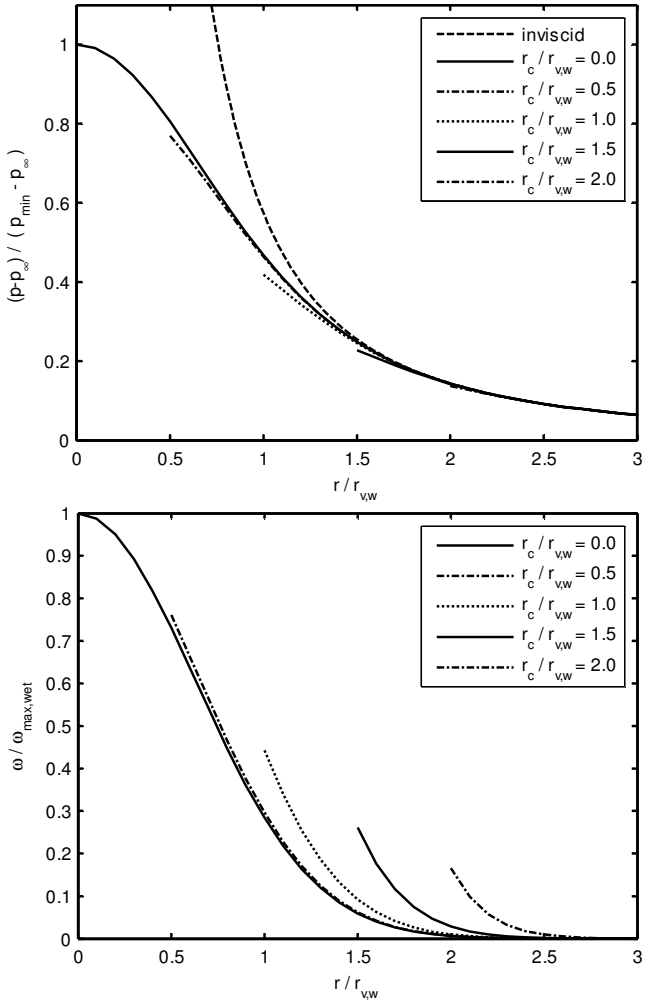

Figure 2: Non-dimensional pressure (top, Eq. (22) divided by Eq. (23)) and vorticity distribution (bottom, Eq. (25)) for various non-dimensional cavity radii.

for arbitrary cavity radius as long as the variation of the cavity radius remains negligible small.

The vorticity and circulation distribution can easily be derived from Eq. (20). The axial vorticity is given by

$$\begin{aligned}\omega_z &= \frac{1}{r}\frac{\partial(rv)}{\partial r} \\ &= \frac{\Gamma_\infty}{\pi}\frac{\zeta}{r_{vw}^2+\zeta r_c^2}\, e^{-\zeta\left(r^2-r_c^2\right)/r_{vw}^2}\end{aligned} \tag{25}$$

and the circulation distribution is given by

$$\Gamma = \Gamma_\infty\left[1-\frac{r_{vw}^2}{r_{vw}^2+\zeta r_c^2}\, e^{-\zeta\left(r^2-r_c^2\right)/r_{vw}^2}\right] \tag{26}$$

The vorticity has its maximum at the edge of the cavitating vortex with its value decreasing with increasing cavity size. The circulation at the edge is now finite.

The angular impulse for two-dimensional axi-symmetric flow is given by

$$\begin{aligned}L &= \rho\iint_S vr\, dS = 2\pi\rho\int_{r_c}^{R} vr^2\, dr \\ &= \rho\Gamma_\infty\left[\tfrac{1}{2}\left(R^2-r_c^2\right)-\frac{r_{vw}^2}{2\zeta}\frac{r_{vw}^2}{r_{vw}^2+\zeta r_c^2}\right]\end{aligned} \tag{27}$$

where it has already been assumed that R is large. It is seen that angular impulse is not well defined as it becomes infinite when R goes to infinity. A quantity that is well defined for two-dimensional flow is the vortical angular impulse, Lamb (1932) [12], art. 152, which is defined as

$$A_z = -\rho\iint_S r^2\omega_z\, dS = -\rho\int_{r_c}^{\infty} 2\pi r^3\omega_z dr \tag{28}$$

and where the relation between the two impulses is given by

$$L = 2\pi\rho \int_{r_c}^{R} v\, r^2 dr = \pi\rho\, v r^3 \Big|_{r_c}^{R} - \frac{A_z}{2} \tag{29}$$

The vortical angular impulse for cavitating flow can be analyzed by substituting Eq. (25) in (28) and is given by

$$A_z = -\frac{\rho \Gamma_\infty r_{vw}^2}{\zeta} \tag{30}$$

from which it is concluded that it is identical for non-cavitating and cavitating flow, but it is not conserved in time due to dissipation by the viscous stresses. The reduction in angular impulse due to cavitation is given by the lower boundary of the first term in the right-hand-side of Eq. (29) or from Eq. (27) and is given by

$$\Delta L = -\pi\rho v_c r_c^3 = -\frac{\rho\zeta\Gamma_\infty}{2} \frac{r_c^4}{r_{vw}^2 + \zeta r_c^2} \tag{31}$$

If the outer boundary R is a factor 10 larger than the radius of the viscous core and the cavity, the reduction in angular impulse due to viscosity is on the order of 2% and it is only on the order of 0.5% due to the presence of the cavity.

Example results are presented in Figure 1 and 2 showing a comparison between an inviscid and viscous non-cavitating vortex and a viscous cavitating vortex for different cavity radii. All radii are made non-dimensional using the viscous core size for non-cavitating flow r_{vw}. The circumferential velocity, made non-dimensional using the velocity at the viscous core for non-cavitating (wetted) flow v_{vw}, is only changed near the cavity to satisfy the boundary condition that the shear stress equals zero and is always smaller for a cavitating vortex. The pressure distribution is presented in Figure 2 from which it seen that the presence of a cavity has a very small influence. The vorticity distribution, presented in Figure 2, shows that vorticity increases near the cavity such that the vortical angular impulse remains constant.

The presented formulations can also be used to define a relation between cavity radius and cavitation number. Kuiper (1981) [7] has determined the cavity size of a propeller tip vortex by analyzing photographs. The propeller (designated propeller V) was operating in open water conditions for a range of cavitation numbers and for two different shaft rotation rates resulting in two different Reynolds numbers. The advance ratio was fixed to a value of 0.4. A comparison between the experimental data and the results of the analytical model is presented in Figure 3. The value for the circulation of the analytical solution and the values of the viscous core are obtained from a fit to the experimental data as no further information is available. The comparison can therefore only be judged from a qualitative point of view. The results show that the slope of the curve depends on the size of the cavity and the size of the viscous core and that there is a region that matches the slope of the experimental results quite well. An increase in Reynolds number is known to lead to a reduction of the viscous core radius. At identical loading and cavitation number this will result in a larger cavity size which is observed in both

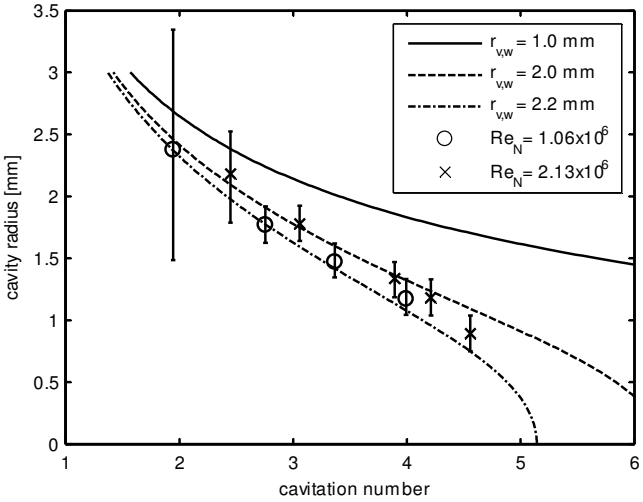

Figure 3: Variation of cavity radius with cavitation number for varying viscous core sizes and comparison with the experimental data of Kuiper (1981) [6], symbols. The circulation and viscous core size for the analytical formulation are fitted.

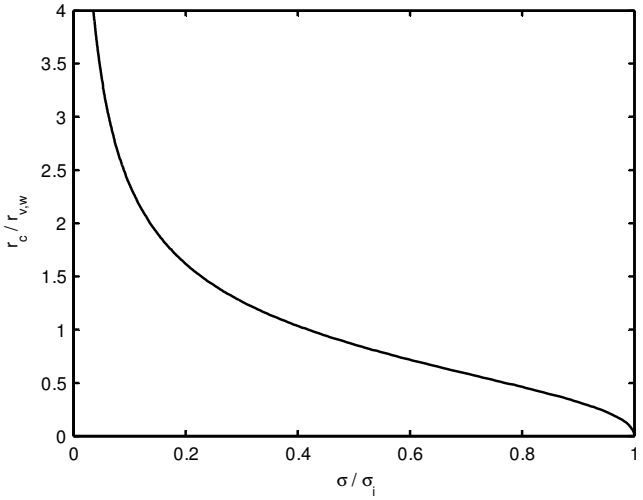

Figure 4: Unique relation between non-dimensional cavity radius and cavitation number for the cavitating Lamb-Oseen vortex.

experiment and theory. When the cavity size becomes much larger than the viscous core size, the influence of viscous effects becomes very small.

The relation between cavity radius and cavitation number is transformed into a single curve by dividing the cavity radius by the viscous core radius and the cavitation number σ by the cavitation number at inception σ_i, which is equivalent to dividing Eq. (22) by Eq. (23). The result is presented in Figure 4. Comparison with the data of Souders & Platzer presented in [8] using a single tuned value for the viscous core radius gives good correlation for small cavity radii. However, when the cavity radius becomes larger than the viscous core radius the correlation becomes worse which is probably related with an incorrect description of the outer circumferential velocity profile by the Lamb-Oseen vortex.

COMPUTATIONAL SOLUTION

The second part of the paper discusses results obtained from a computational model that directly solves Eq. (1) through (3) without further simplifications. An analytical solution can be derived for the radial velocity distribution by combining Eq. (1) with (13) which gives

$$u = \frac{\dot{r}_c\, r_c}{r} \tag{32}$$

where $\dot{r}_c$ corresponds to the time derivative of the cavity radius. The system of equations can be simplified by using the following coordinate transformation proposed by Chahine (1995) [11]

$$s = \frac{r}{r_c} \tag{33}$$

which is valid as long as there is no collapse of the cavity. The radial and circumferential momentum equations are then given by[1]

$$\begin{aligned} r_c \ddot{r}_c + \dot{r}_c^2 = {} & \frac{\dot{r}_c^2}{2\ln s_\infty}\left[-s_\infty^{-2}+1\right] + \frac{1}{\ln s_\infty}\int_1^{s_\infty} \frac{v^2}{s}\, ds \\ & - \frac{1}{\rho \ln s_\infty}\left[p_\infty - p_c\right] \end{aligned} \tag{34}$$

$$\frac{dv}{dt} = \frac{s\dot{r}_c}{r_c}\frac{\partial v}{\partial s} - \frac{\dot{r}_c}{r_c s}\left(\frac{\partial v}{\partial s} + \frac{v}{s}\right) + \frac{\mu}{\rho r_c^2}\left(\frac{\partial^2 v}{\partial s^2} + \frac{1}{s}\frac{\partial v}{\partial s} - \frac{v}{s^2}\right) \tag{35}$$

where the radial momentum equation is integrated over the computational domain $[1, s_\infty]$. In the derivation of Eq. (35) use has been made of the time derivative following the grid motion

$$\frac{dv}{dt} = \frac{\partial v}{\partial t} + \frac{\partial v}{\partial r}\frac{\partial r}{\partial t} = \frac{\partial v}{\partial t} + \frac{\partial v}{\partial s}\frac{s\dot{r}_c}{r_c} \tag{36}$$

which accounts for the change in radial location of the grid coordinates prescribed in the s-coordinate system.

The boundary conditions at the cavity surface as given by Eq. (14) and (15) are then given by:

$$p_c = p_v - 2\mu\frac{\dot{r}_c}{r_c} \tag{37}$$

$$\frac{\partial v_c}{\partial s} = v_c \tag{38}$$

where the influence of surface tension and non-condensable gas has been neglected. At the outer edge of the domain the circumferential velocity is prescribed by the potential flow solution Eq. (8) in the grid-coordinate system

[1] Note that the sign of the first term in the right-hand-side of Eq. (35) is opposite to the formulation presented in [11].

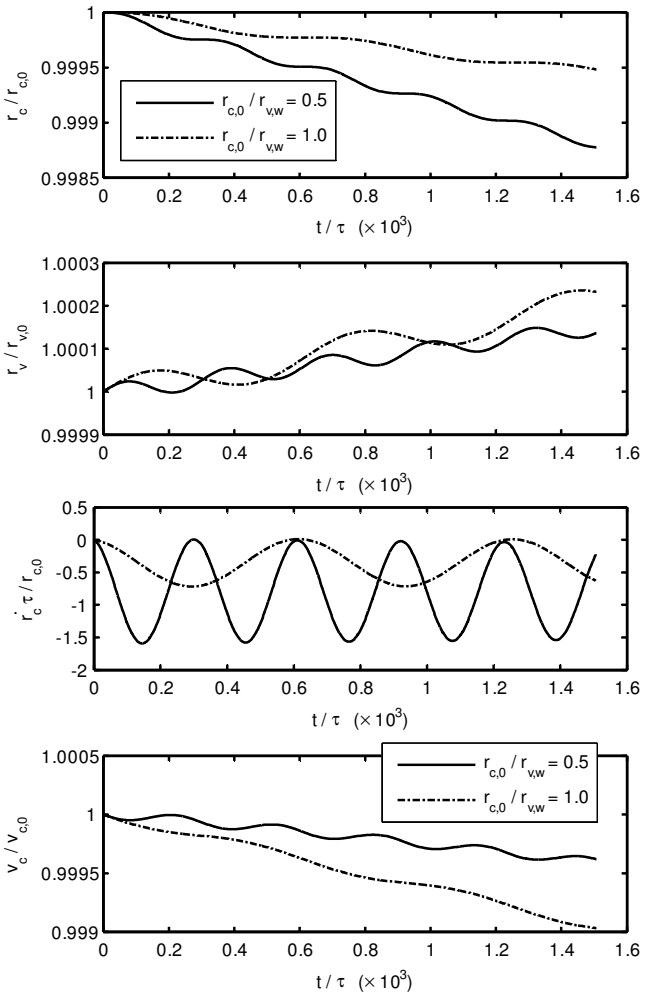

Figure 5: Unsteady behavior of cavity and circumferential flow for constant pressure difference with the outer boundary located at $r_\infty / r_{vw} = 500$ for the first time step.

$$v_\infty = \frac{\Gamma_\infty}{2\pi r_c s_\infty} \tag{39}$$

In the computations two different cases will be distinguished. In the first case the pressure p_{ref} will be prescribed and fixed in time and the pressure at the outer boundary is given by

$$p_\infty = p_{\text{ref}} - \tfrac{1}{2}\rho\left(v_\infty^2 + \left(\dot{r}_c / s_\infty\right)^2\right) \tag{40}$$

In the second case the motion of the cavity will be prescribed and no additional boundary condition for the outer edge is required. For the initial condition the analytical solution for the stationary vortex ($\dot{r}_c = 0$) described in the previous section is used. The non-linear system of equations is discretized in time using a Crank-Nicholson scheme, in space using second order accurate difference schemes and iteratively solved using a Newton method and a direct solver.

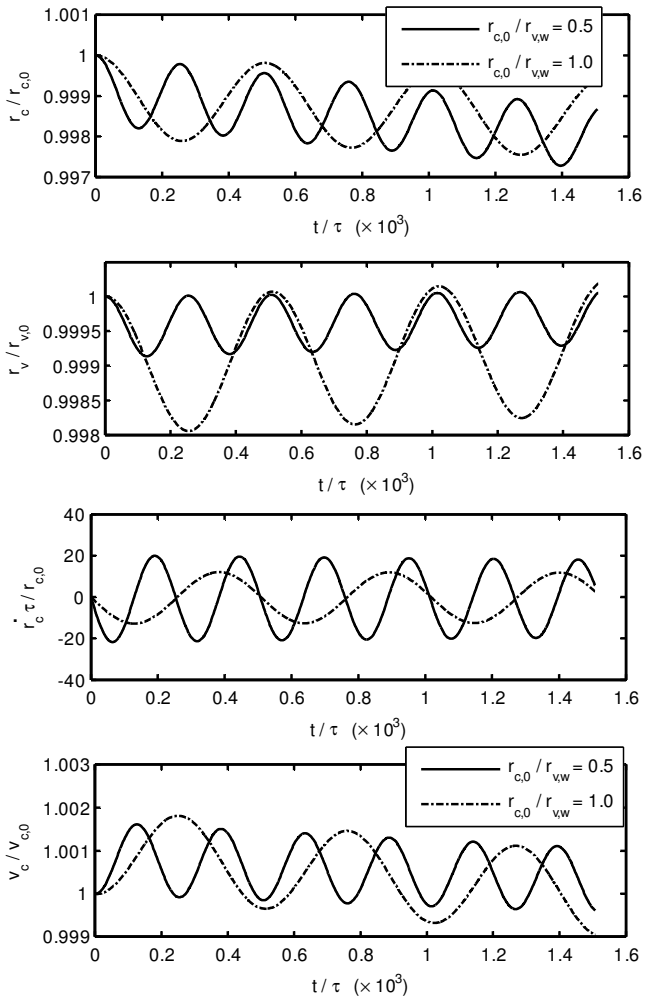

Figure 6: Unsteady behavior of cavity and circumferential flow for constant pressure difference with the outer boundary located at $r_\infty / r_{vw} = 50$ for the first time step.

Substitution of the viscous boundary condition Eq. (38) at the cavity core s=1 in Eq. (35) leads to the following equation for the change in circumferential velocity at the cavity

$$\frac{dv_c}{dt} = -v_c \frac{\dot{r}_c}{r_c} + \frac{\mu}{\rho r_c^2} \frac{\partial^2 v_c}{\partial s^2} \tag{41}$$

For the analytical solution, valid for constant cavity radius, the first term in the right-hand-side is always zero and the second derivative of the velocity with respect to s is always negative, hence the diffusion term leads to a reduction of the velocity at the edge of the cavity. However, for rapid changes in cavity radius, the first term in the right-hand side will dominate and the circumferential velocity near the cavity depends on the change in cavity size. It will increase when the cavity radius decreases with time.

The velocity for the inviscid part of the vortex is described by the potential flow solution Eq. (8) and the change in velocity as given by Eq. (35) is given by

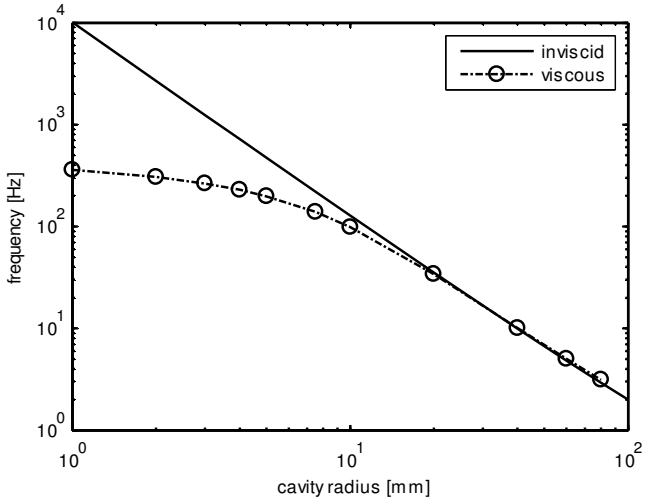

Figure 7: Variation of the computed resonance frequency with cavity radius and comparison with the inviscid flow solution given by Eq. (43). The viscous core radius equals $r_v = 10\,\text{mm}$.

$$\frac{dv}{dt} = \frac{s\dot{r}_c}{r_c} \frac{\partial v}{\partial s} \tag{42}$$

Comparison with Eq. (36) then shows that the partial derivative with respect to time equals zero which implies that the cavity dynamics will not lead to a change in the circumferential velocity distribution of the potential flow.

COMPUTATIONAL SOLUTION: RESULTS

For a first analysis of the equations, the pressure difference $(p_{ref} - p_v)$ is kept constant and is computed from Eq. (34) combined with Eq. (37) and (40) using the prescribed initial velocity distribution and assuming a stationary vortex ($\dot{r}_c = \ddot{r}_c = 0$). Hence the driving mechanism for unsteady behavior is diffusion. The cavity response and the circumferential velocity are computed by simultaneously solving Eq. (34) and Eq. (35). The circumferential velocity is given by Eq. (20) with $\Gamma_\infty = 1.0\,\text{m}/\text{s}^2$ and $r_{vw} = 10\,\text{mm}$. The influence of the location of the outer boundary r_∞ is investigated by comparing the solution for two locations, being $r_\infty / r_{vw} = 500$ and $r_\infty / r_{vw} = 50$ for the initial solution. The two different locations of the outer boundary leads to a 0.1% difference in $(p_{ref} - p_v)$ due to numerical errors in evaluating the integral of Eq. (34). In the computations the domain size $s_\infty = r_\infty / r_{c,0}$ is fixed with $r_{c,0}$ the cavity size of the initial solution. Hence, any change in r_c leads to a change in r_∞. A parameter study showed that grid and time step independent solutions were obtained for 200 vertices and a time step of 10 µs. Density and kinematic viscosity are given by $\rho = 1000\ \text{kg/m}^3$ and $\nu_l = 10^{-6}\,\text{m}^2/\text{s}$, respectively.

Results for two different initial cavity radii are presented in Figure 5 and 6. The location of the cavity and the viscous core

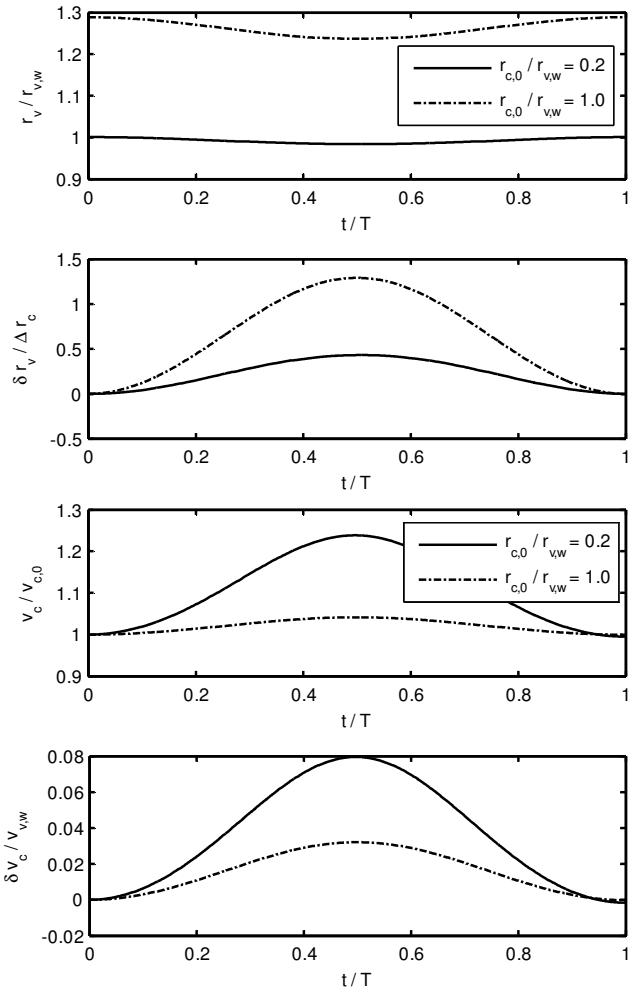

Figure 8: Non-dimensional results for a forced unsteady cavity motion for two different cavity sizes. Presented are, from top to bottom, viscous core radius, change in viscous core radius, circumferential velocity at cavity and change in circumferential velocity at cavity.

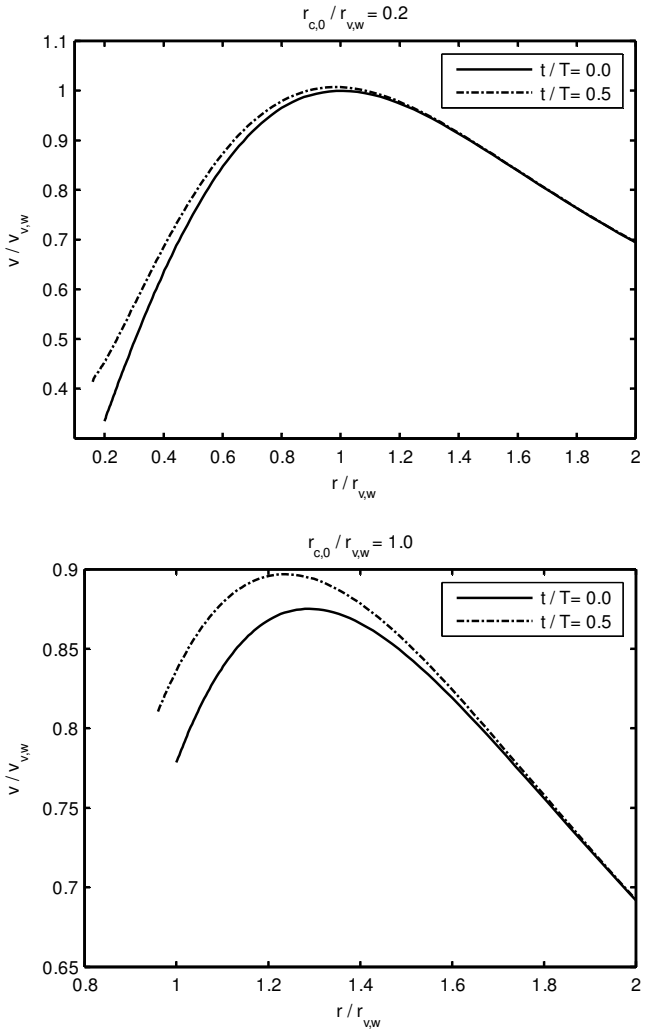

Figure 9: Non-dimensional circumferential velocity distribution at two time steps for the cavity motion presented in Figure 8.

and the circumferential velocity at the core are made non-dimensional by the corresponding value of the initial solution. The viscous core radii r_v and $r_{v,0}$ correspond to the actual location with maximum velocity of a parabola fitted through 3 grid points around the point with the maximum circumferential velocity. The time is made non-dimensional with a time scale related to diffusion given by $\tau = r_{vw}^2 / (4\zeta\nu_l) = 19.9$ s. As expected, the diffusion causes an increase of the viscous core. The change in cavity is accompanied by oscillations, of which the frequency depends on cavity size and location of the outer boundary. The smaller boundary size also amplifies the oscillations. During the oscillatory period a reduction in cavity size is accompanied with an increase of the velocity near the cavity according to Eq. (41). The diffusion leads to a reduction of the cavity size instead of an increase which was suggested by the analytical solution. This reduction is caused by the constant pressure difference $(p_{ref} - p_v)$ which is forced in the computational solution but which is violated by the analytical solution. A reduction of the cavity size with downstream distance (or time) was also observed in [6] for the cavitating vortex of a propeller operating in a cavitation tunnel. The viscous core radius follows the oscillatory motion of the cavity as also shown in [11].

The influence of the cavity radius on the resonance frequency is further analyzed by varying the cavity radius $r_{c,0}/r_{vw}$ between 0.1 and 8.0 with domain size $r_\infty/r_{vw} = 50$. A comparison is made with the resonance frequency for inviscid flow, obtained from Eq. (34) by assuming a small harmonic perturbation of the cavity radius and using Eq. (8) for the velocity distribution. Considering only the linear term, gives the following relation for the resonance frequency f in Hz

$$2\pi f = \frac{\Gamma_\infty}{2\pi r_c^2}\sqrt{\ln^{-1}\frac{r_\infty}{r_c}} \qquad (43)$$

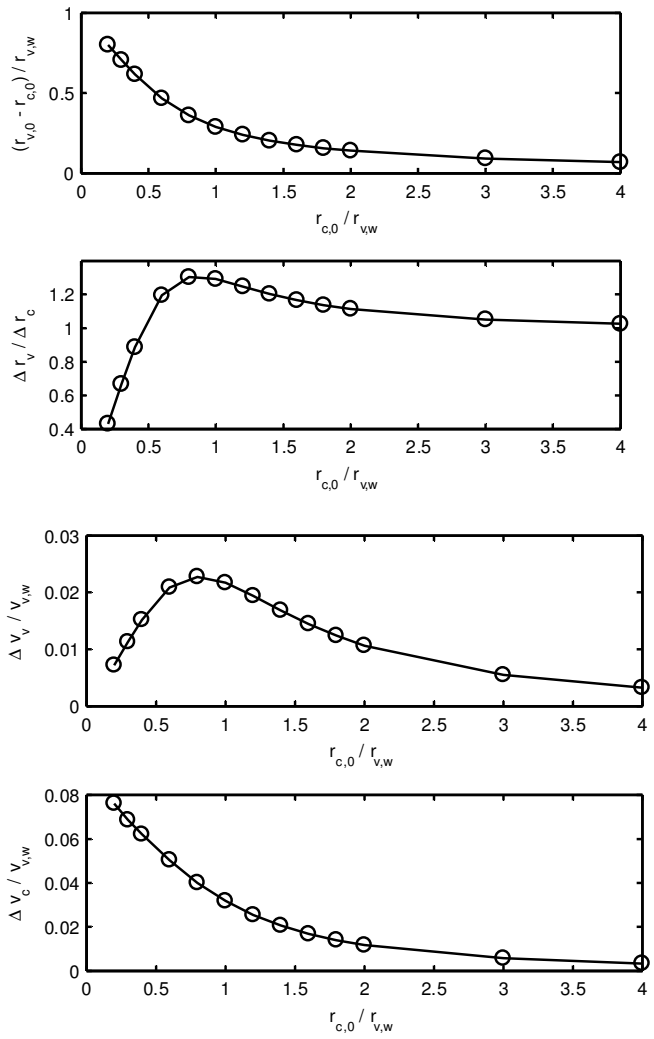

Figure 10: Results for a forced unsteady cavity motion for varying initial cavity radius $r_{c,0}$. Presented are, from top to bottom, distance between initial viscous core radius and cavity radius, relative amplitude of viscous core position, relative maximum change of circumferential velocity at the viscous core radius and the relative maximum change of circumferential velocity at the cavity.

Results are presented in Figure 7. Viscous effects reduce the value of the resonance frequency if the cavity radius becomes smaller than the viscous core radius. The viscous flow computations suggest that the resonance frequency asymptotically approaches a constant value with decreasing cavity size. The dependency of this limiting value on parameters like circulation and viscous core size needs to be further investigated.

The resonance frequency for inviscid flow as given by Eq. (43) shows a dependency on the location of the outer boundary r_∞. The same dependency is expected for viscous flow which explains the differences in oscillation period observed between Figure 5 and Figure 6. The increase in amplitude of the cavity motion with smaller radius of the outer boundary is probably related to the logarithm in the right-hand-side of Eq. (34) which scales the difference between the velocity integral and the pressure difference.

In the second series of computations, the radius of the cavity is fully prescribed in time, which physically corresponds to prescribing the radial velocity component at the edge of the domain. The circumferential velocity is then obtained by solving Eq. (35) after which the pressure at the outer boundary can be computed from Eq. (34). The cavity radius is prescribed by

$$r_c = r_{c,0} - 0.5\Delta r_c\left[1-\cos\left(2\pi t/T\right)\right] \tag{44}$$

The peak-peak value and period equal $\Delta r_c / r_{vw} = 0.04$, $T = 1\,\mathrm{ms}$, respectively. The circulation and viscous core size are as given previously which results into $\dot{r}_{c,\max} / v_{vw} = 0.11$. The number of vertices is increased to 400 and 1000 timesteps are used in one period. The size of the domain equals $r_\infty / r_{vw} = 500$. The period is small enough such that diffusion has no influence on the results.

Typical results for the time variation for two cavity sizes are presented in Figure 8 and the minimum and maximum velocity distributions are presented in Figure 9. The symbol δ corresponds to the local change while Δ corresponds to the maximum change. The variation of various quantities is given in Figure 10 as a function of non-dimensional initial cavity radius. The difference between the initial viscous core size and the cavity size decreases exponentially with increasing cavity size and is given by the analytical solution. The amplitude of the viscous core radius is somewhat larger than the cavity radius as long as the cavity is larger than approximately 50% of the viscous core. The amplitude of the viscous core radius has a maximum when the cavity size equals the viscous core size and decreases rapidly for smaller cavity sizes. The amplitude of the circumferential velocity at the viscous core has a similar trend as the viscous core size and has its maximum when the initial cavity size is slightly smaller than the non-cavitating viscous core size. The change in maximum circumferential velocity at the cavity however increases very rapidly when the cavity becomes smaller. The same trend is observed from the first term in the right-hand-side of Eq. (41) when using Eq. (21) for the circumferential velocity. Both maximum changes in velocity have been non-dimensionalized using the maximum circumferential velocity for the non-cavitating flow. The changes also depend on the cavity velocity $\dot{r}_c$ which has been kept constant in all simulations.

The two computational cases presented here are focused on unsteady cavity behavior using the analytical solution as the initial solution. If the temporal behavior of the analytical solution is to be reproduced by the computations, the cavity radius should be prescribed by Eq. (19) with the condition that the radial velocity component given by Eq. (24) has to remain small which implies a restriction on the maximum cavity radius with respect to the viscous core radius. This has not been further investigated.

CONCLUSIONS

The structure of an axi-symmetric cavitating vortex in two-dimensional, unsteady, incompressible and viscous flow has been analyzed. The applied boundary condition for the velocity at the cavity corresponds to a zero shear stress condition. Neglecting the radial velocity component, corresponding to a stationary cavity, allows for the generation of an analytical solution for the circumferential velocity and the pressure distribution. In addition, a computational model has been developed that solves the system of equations without further simplifications.

The analytical solution shows that the circumferential velocity of a cavitating vortex is always smaller than that of a non-cavitating vortex. The change in velocity is occurring in a small region just outside the cavity of which the size exponentially decreases with increasing cavity size. It is shown that the vortical angular impulse does not change with varying cavity size but the angular impulse is slightly reduced due to the presence of the cavity.

The analytical solution is derived for unsteady flow and suggests an increase in viscous core size and cavity size under influence of diffusion. There is however no constant pressure difference between the cavity and the outer boundary. The computational solution shows that with constant pressure difference the viscous core size increases but the cavity size decreases due to diffusion, as observed in experiment. This shows that the analytical solution can only be used to give a local description of a stationary cavity.

The size of the viscous core has a small influence on the cavity size at given cavitation number if the cavity is much larger than the viscous core but it has a significant influence if the cavity size is of the same order or smaller than the viscous core. A larger viscous core leads to a reduction of the cavity size. This trend is also observed in experimental data and is expected to be generally valid. The analytical model has its limitations in the sense that it is only valid for vortices of which the circumferential velocity is described by a Lamb-Oseen vortex, which is not very often. Extension towards more general velocity distributions such as used in [8] should be pursued.

The unsteady computations show oscillations of the cavity radius from which a resonance frequency could be determined. Computations show that viscous effects lead to a reduction of the resonance frequency if the cavity size becomes smaller than the viscous core size and suggest that the resonance frequency has a limiting value when cavity size approaches zero. A similar behavior is expected for three-dimensional volume oscillations of the cavity which will improve the correlation in resonance frequency between theory and experiment for small cavity sizes or large cavitation numbers presented in [4].

The unsteady computations show that the circumferential velocity at the cavity increases when the cavity radius decreases. However, after collapse the circumferential velocity at the center should be zero and it is thus expected that a reduction of the circumferential velocity will occur in the last phase of the collapse where viscous effects become dominant. This part of the collapse cannot be modeled with the applied coordinate transformation but is currently under investigation using a modified computational model.

REFERENCES

[1] Bosschers, J, 2009, "Investigation of hull pressure fluctuations generated by cavitating vortices", *First International Symposium on Marine Propulsors, smp'09*, Trondheim, Norway.

[2] Keller, J.J. and Escudier, M.P., 1980, "Theory and observations of waves on hollow-core vortices", *J. Fluid Mechanics*, Vol. 99, part 3, pp. 495-511.

[3] Maines, B. and Arndt, R.E.A., 1997, "The case of the singing vortex", *Journal of Fluids Engineering*, Vol. 119, p. 271-276.

[4] Bosschers, J., 2008, "Analysis of inertial waves on inviscid cavitating vortices in relation to low-frequency radiated noise", *WIMRC Cavitation Forum*, Warwick University, UK.

[5] Falcão de Campos, J.A.C., 1992, "Laser-Doppler velocity measurements on tip vortices in non-cavitating and cavitating conditions", ASME FED-Vol. 135 *Cavitation and multiphase flow Forum*.

[6] van Rijsbergen, M.X. and Kuiper, G., 1997, "Modeling a cavitating vortex", *ASME* FEDSM'97-3266.

[7] Kuiper, G., 1981, *Cavitation inception on ship propeller models*, PhD thesis, Delft University of Technology.

[8] Arakeri, V.H., Higuchi, H. and Arndt, R.E.A., 1988, "A model for predicting tip vortex cavitation characteristics", *J. of Fluids Engineering*, Vol. 110, pp. 190-193.

[9] Choi, J. and Ceccio, S.L., 2007, "Dynamics and noise emission of vortex cavitation bubbles", *J. Fluid Mechanics*, Vol. 575, pp. 1-26.

[10] Bosschers, J., Janssen, A.A. and Hoeijmakers, H.W.M., 2008, "Similarity solutions for viscous cavitating vortex cores". *Journal of Hydrodynamics,* Vol. 20, No. 6, pp. 689-688.

[11] Chahine, G.L., 1995, "Bubble interactions with vortices", in Green, S. L., *Fluid Vortices,* Kluwer Academic Publishers, Dordrecht, The Netherlands

[12] Lamb, H., 1932, *Hydrodynamics*, 6th Edition, Cambridge University Press.

[13] Newman, B.G., 1959, "Flow in a viscous trailing vortex", *Aeronautical Quarterly*, Vol. 10, No. 2, pp. 167-188.